Journal of Ginseng Research 46 (2022) 357–366

Contents lists available at ScienceDirect

Journal of Ginseng Research

journal homepage: https://www.sciencedirect.com/journal/journal-of-ginseng-research

Research Article

Identification of anti-adipogenic withanolides from the roots of Indian ginseng (*Withania somnifera*)

Seoung Rak Lee [a, b], Bum Soo Lee [a], Jae Sik Yu [a], Heesun Kang [a], Min Jeong Yoo [a], Sang Ah Yi [a], Jeung-Whan Han [a], Sil Kim [a], Jung Kyu Kim [c], Jin-Chul Kim [d], Ki Hyun Kim [a, *]

[a] School of Pharmacy, Sungkyunkwan University, Suwon, Republic of Korea
[b] Department of Chemistry, Princeton University, NJ, United States
[c] School of Chemical Engineering, Sungkyunkwan University, Suwon, Republic of Korea
[d] KIST Gangneung Institute of Natural Products, Natural Product Informatics Research Center, Gangneung, Republic of Korea

ARTICLE INFO

Article history:
Received 4 February 2021
Received in revised form
17 September 2021
Accepted 30 September 2021
Available online 6 October 2021

Keywords:
Indian ginseng
Withanolides
NMR chemical Shift calculations
3T3-L1 preadipocytes
Adipogenesis

ABSTRACT

Background: *Withania somnifera* (Solanaceae), generally known as Indian ginseng, is a medicinal plant that is used in Ayurvedic practice for promoting health and longevity. This study aims to identify the bioactive metabolites from Indian ginseng and elucidate their structures.
Methods: Withanolides were purified by chromatographic techniques, including HPLC coupled with LC/MS. Chemical structures of isolated withanolides were clarified by analyzing the spectroscopic data from 1D and 2D NMR, and HR-ESIMS experiment. Absolute configurations of the withanolides were established by the application of NMR chemical shifts and ECD calculations. Anti-adipogenic activities of isolates were evaluated using 3T3-L1 preadipocytes with Oil Red O staining and quantitative real-time PCR (qPCR).
Results: Phytochemical examination of the roots of Indian ginseng afforded to the isolation of six withanolides (**1**–**6**), including three novel withanolides, withasilolides G–I (**1**–**3**). All the six compounds inhibited adipogenesis and suppressed the enlargement of lipid droplets, compared to those of the control. Additionally, the mRNA expression levels of *Fabp4* and *Adipsin*, the adipocyte markers decreased noticeably following treatment with 25 μM of **1**–**6**. The active compounds (**1**–**6**) also promoted lipid metabolism by upregulating the expression of the lipolytic genes *HSL* and *ATGL* and downregulating the expression of the lipogenic gene *SREBP1*.
Conclusion: The results of our experimental studies suggest that the withasilolides identified herein have anti-adipogenic potential and can be considered for the development of therapeutic strategies against adipogenesis in obesity. Our study also provides a mechanistic rationale for using Indian ginseng as a potential therapeutic agent against obesity and related metabolic diseases.

1. Introduction

Withania somnifera (Solanaceae), widely recognized as Indian ginseng and ashwagandha, is widely distributed in the dry regions of India, Sri Lanka, South Africa, and the Mediterranean [1,2]. Indian ginseng has been used as a functional food for promoting health and longevity via activation of the immune system against diseases, revitalizing the organ systems in weakened conditions, and curbing the process of aging [2,3]. As it is medically safe to use Indian ginseng, the herb has been used for a long time by people of all ages and sexes, and even during pregnancy, and has not been reported to produce any side effects [3,4]. Indian ginseng is commercially cultivated in the Indian states of Uttar Pradesh, Madhya Pradesh, Punjab, and Gujarat, and India is exporting the roots of this herb to other countries [5]. The herb is commonly known as rasayana in Ayurvedic practice. As the Queen of Indian herbs, the roots of Indian ginseng have been traditionally used in Indian Ayurveda as a tonic for vitality, longevity, and the maintenance and restoration of health [6]. As these properties are quite similar to those of ginseng, *W. somnifera* is also referred to as Indian ginseng [7]. The herb has been widely used for therapeutic purposes owing to its anti-oxidative, analgesic, antiepileptic, antiulcerative, and antibacterial

* Corresponding author. School of Pharmacy, Sungkyunkwan University, Suwon, 16419, Republic of Korea.
E-mail address: khkim83@skku.edu (K.H. Kim).

https://doi.org/10.1016/j.jgr.2021.09.004

properties [8]. Pharmacological and clinical studies have shown that this plant can be used for treating anxiety, cognitive and neurological disorders, inflammatory diseases, hyperlipidemia, and Parkinson's disease [9–11]. Interestingly, Indian ginseng has also been prescribed for alleviating tolerance and chronic dependence on various psychotropic medications [12]. Phytochemical studies on this herb have reported the presence of biologically active chemical constituents, including alkaloids, steroids, saponins and withanolides, having diverse pharmacological properties [13–15]. The main metabolites of Indian ginseng are alkaloids and steroidal lactones, known as withanolides, which are the most important constituents responsible for the medicinal properties of Indian ginseng [16]. It has been reported that the herb also contains other chemical metabolites, including acylsteryl glucosides, starch, reducing sugars, hantreacotane, ducitol, and various amino acids [13–15]. Withaferin A, one of the most representative withanolides found in *W. somnifera* has been reported to exhibit anti-tumor effects including pro-apoptotic and anti-angiogenesis activity [17]. Recently, withaferin A was also found to show anti-adipogenesis effects in 3T3-L1 adipocytes by reducing lipid accumulation and downregulating the expression of key activators of adipogenesis, peroxisome proliferator-activated receptor gamma (PPARγ) and CCAAT/enhancer binding protein alpha (C/EBPα) as well as adipocyte fatty acid binding protein [17]. Despite the high nutritive and therapeutic values of Indian ginseng, there are few reports on the phytochemical investigation of the bioactive constituents of Indian ginseng. Therefore, we aimed to discover the bioactive metabolites in this promising natural source in this study.

In our ongoing endeavors to identify structurally and/or bioactive metabolites from a variety of natural sources [18–21], we conducted a phytochemical exploration of the MeOH extracts of the Indian ginseng (*W. somnifera*) roots. We have previously identified numerous secondary metabolites, including 13 withanolides, 5 phenolic compounds, and 1 alkaloid by phytochemical examination of the MeOH extracts of Indian ginseng. Of these metabolites, 6 were novel withanolides (withasilolides A–F), and 4 of these withasilolides showed cytotoxicity against several human cancer cells including SK-MEL-2, HCT-15, A549 and SK-OV-3) [22]. We also identified new phenylpropanoid esters, namely withaninsam A and withaninsam B, in addition to phenolic compounds and alkaloids with anti-inflammatory potential [23]. In this study, we further performed the phytochemical analysis of Indian ginseng coupled with the liquid chromatography/mass spectrometry (LC/MS) for identifying the novel bioactive metabolites in Indian ginseng. Our analyses afforded to the isolation and structural elucidation of 3 novel withanolides (**1**–**3**) and 3 known compounds (**4**–**6**). The chemical structures of three new withanolides were verified by interpretation and analysis of the data obtained by 1D and 2D NMR data, high-resolution mass spectrometry, gauge-including atomic orbital (GIAO) nuclear magnetic resonance (NMR) chemical shift and electronic circular dichroism (ECD) calculations. This study describes the separation/isolation and chemically structural determination of all the isolated withanolides (**1**–**6**) along with their effects on *de novo* adipogenesis and lipid metabolism in 3T3-L1 adipocytes.

2. Materials and methods

2.1. General experimental procedure and plant material

The related information was included in Supplementary materials.

2.2. Extraction and separation/isolation

The dried and crushed roots (1.1 kg) of *W. somnifera* were extracted using 80% MeOH (3.0 L × 3 days) under reflux and filtered. Resultant filtrate was evaporated *in vacuo* to generate 180 g of crude MeOH extract, which was directly dissolved in 700 mL distilled H_2O and then solvent-partitioned with hexane, dichloromethane, ethyl acetate, and butanol, yielding 3.1, 4.2, 1.9, and 17.8 g of residue, respectively. The LC/MS analysis was performed using an in-house-built UV spectra library, and the results revealed that the withanolides were mainly present in the dichloromethane-soluble fraction. The isolation procedure to obtain the compounds **1**–**6** from dichloromethane fraction was described in Supplementary materials.

2.2.1. Withasilolide G (*1*)

White powder; $[\alpha]_D^{25}$-27.1 (*c* 0.11, methanol); UV (methanol) λ_{max} (log ε) 220 (3.4) nm; IR (KBr) ν_{max} 3716, 2977, 2841, 2502, 1718, 1524, and 1032 cm^{-1}; ECD (methanol) λ_{max} ($\triangle\varepsilon$) 216 (−1.1), 260 (+2.1), and 304 (−4.6) nm; ^1H and ^{13}C NMR (800 MHz and 200 MHz, respectively), refer Table 1; positive HR-ESIMS *m/z* 455.2785 $[M + H]^+$ (calculated for $C_{28}H_{39}O_5$, 455.2797).

2.2.2. Withasilolide H (*2*)

White powder; $[\alpha]_D^{25}$+39.3 (*c* 0.15, methanol); UV (methanol) λ_{max} (log ε) 230 (2.9) nm; IR (KBr) ν_{max} 3713, 3330, 2957, 1760, 1459, 1133, and 1038 cm^{-1}; ECD (methanol) λ_{max} ($\triangle\varepsilon$) 223 (−0.6), 255 (+0.3), and 337 (−4.1) nm; ^1H and ^{13}C NMR (800 MHz and 200 MHz, respectively), refer Table 1; positive HR-ESIMS *m/z* 489.2852 $[M + H]^+$ (calculated for $C_{28}H_{41}O_7$, 489.2852).

2.2.3. Withasilolide I (*3*)

White powder; $[\alpha]_D^{25}$+14.2 (*c* 0.10, methanol); UV (methanol) λ_{max} (log ε) 225 (3.1) nm; IR (KBr) ν_{max} 3713, 2972, 2838, 2497, 1713, 1520, and 1029 cm^{-1}; ECD (methanol) λ_{max} ($\triangle\varepsilon$) 256 (+2.4) and 336 (−3.1) nm; ^1H and ^{13}C NMR (800 MHz and 200 MHz, respectively), refer Table 1; positive HR-ESIMS *m/z* 487.2689 $[M + H]^+$ (calculated for $C_{28}H_{39}O_7$, 487.2696).

2.3. Computational analyses

All the conformers reported in this study were generated using the MacroModel module (version 2019–3, Schrödinger LLC) [24]. The detailed process for geometry optimization was included in Supplementary materials.

The ECD calculations for conformers **1a/2a/3a** and **1b/2b/3b** were conducted at identical theoretical levels and basis sets, the detailed process of which was described in Supplementary materials. The ECD was visualized using SigmaPlot, version 14.0.

The calculations for the optimized conformers of 17*R*-**2**/17*R*-**3** and 17*S*-**2**/17*S*-**3** were performed with GIAO magnetic shielding constants at the B3LYP/6-31 + G(d) level of theory [25]. The detailed process for the NMR chemical shifts calculation was inserted in Supplementary materials.

2.4. Cell culture and cell differentiation

The related information was included in Supplementary materials.

Table 1
^{1}H (800 MHz) and ^{13}C NMR (200 MHz) data of compounds **1**–**3** in $CDCl_3$.[a,b]

Position	1		2		3	
	δ_C	δ_H (*J* in Hz)	δ_C	δ_H (*J* in Hz)	δ_C	δ_H (*J* in Hz)
1	209.6 s		202.9 s		203.0 s	
2α	39.5 t	2.77 dd (20.0, 4.5)	129.0 d	5.82 dd (10.0, 2.5)	128.9 d	5.85 dd (10.0, 2.5)
2β		3.29 dd (20.0, 2.5)				
3	125.6 d	5.79 m	139.7 d	6.57 ddd (10.0, 5.0, 2.0)	139.5 d	6.58 ddd (10.0, 5.0,2.0)
4α	129.1 d	6.07 d (10.5)	36.6 t	2.51 dd (19.0, 5.0)	36.6 t	2.53 dd (19.0, 5.0)
4β				2.65 m		2.68 m
5	144.7 s		73.1 s		73.2 s	
6	127.1 d	5.80 d (4.5)	56.1 d	3.01 d (3.5)	55.9 d	3.05 d (4.0)
7	64.5 d	3.94 m	57.0 d	3.29 dd (3.5, 2.0)	56.8 d	3.35 m
8	36.2 d	1.50 m	35.3 d	1.75 m	36.4 d	1.92 m
9	33.6 d	2.01 m	34.9 d	1.56 m	35.1 d	1.54 m
10	52.8 s		50.9 s		50.9 s	
11α	21.8 t	1.97 m	21.3 t	2.82 m	21.7 t	2.78 m
11β		1.54 m		1.28 m		1.32 m
12α	39.7 t	1.35 m	32.5 t	1.42 m	33.2 t	1.74 m
12β		2.00 m		1.77 m		2.16 m
13	43.3 s		48.1 s		50.5 s	
14	50.1 d	1.51 m	46.0 d	2.24 m	46.6 d	2.00 m
15α	21.6 t	1.97 m	22.3 t	1.90 m	21.5 t	1.56 m
15β		1.54 m		1.29 m		1.40 m
16α	23.7 t	1.23 m	32.2 t	1.64 m	33.4 t	1.74 m
16β		1.79 m		2.32 m		2.35 m
17	54.4 d	1.48 m	89.4 s		87.0 s	
18	13.4 q	0.90 s	16.2 q	0.89 s	17.2 q	1.02 s
19	18.4 q	1.32 s	14.7 q	1.15 s	14.6 q	1.19 s
20	75.5 s		76.0 s		78.1 s	
21	20.7 q	1.27 s	21.9 q	1.24 s	19.9 q	1.37 s
22	80.7 d	4.19 dd (13.5, 3.5)	80.6 d	4.45 dd (11.0, 3.5)	82.3 d	4.63 dd (11.0, 3.0)
23α	31.6 t	2.11 m	30.4 t	1.56 m	31.5 t	2.28 m
23β		2.37 m		2.27 m		2.79 m
24	149.1 s		30.8 d	1.74 m	150.7 s	
25	122.1 s		40.3 d	2.12 dq (9.5, 6.5)	120.9 s	
26	166.3 s		174.4 s		164.8 s	
27	12.3 q	1.86 s	14.0 q	1.21 d (6.5)	12.1 q	1.87 s
28	20.4 q	1.93 s	20.9 q	1.11 d (7.0)	20.5 q	1.97 s

[a] The coupling constants (in parentheses) are in Hz.
[b] The ^{13}C NMR data were assigned on the basis of the data obtained in the HSQC and HMBC experiments.

2.5. Oil Red O staining

The staining of lipid droplets in the differentiated adipocytes was conducted using Oil Red O working solution for visualization, the procedure of which was described in Supplementary materials in detail.

2.6. Cell viability

The 3T3-L1 preadipocytes were seeded in 6-well plates and treated with compounds **1**–**6** at concentrations of 12.5 and 25 μM for 24 h. The cells were detached with trypsin/EDTA solution (TE) and diluted with PBS. Counting of the number of cells was conducted using an equipment of LUNA-II™ Automated Cell Counter (Logos Biosystems).

2.7. Reverse transcription and quantitative real-time PCR (RT-qPCR)

In order to extract the total RNA from the mature adipocytes, we used the Easy-Blue reagent (Intron Biotechnology, Seongnam, Korea) based on the manufacturer's instructions. The related process was included in Supplementary materials in detail.

2.8. Statistical analyses

All the results and data presented as the standard error of the mean (SEM) for n = 3. Statistical significance was analyzed using Student's *t*-test (two-tailed) in Excel and was assessed on the basis of the *P*-value (*P < 0.05, **P < 0.01, ***P < 0.001 vs. the control group).

3. Results and discussion

3.1. Compound isolation

LC/MS-based examination of the solvent-partitioned fractions from the Indian ginseng extracts combined with our in-house UV library revealed that the CH_2Cl_2-soluble fraction was rich in withanolides. This led to an intensive phytochemical exploration of the fraction using successive column chromatographic purification and preparative and semi-preparative HPLC, which afford to the isolation of 6 withanolides (**1**–**6**), of which 3 were identified as novel withanolides (**1**–**3**) (Fig. 1A).

3.2. Structural identification of the compounds

Compound **1** was separated as a white powder. The molecular formula of **1** was deduced to be $C_{28}H_{38}O_5$, based on the data obtained from NMR (Table 1) and positive-ion mode HR-ESIMS, which displayed one protonated ion peak at *m/z* 455.2785 $[M + H]^+$ (calculated for $C_{28}H_{39}O_5$, 455.2797). The UV data of **1** displayed a distinctive feature at λ_{max} 220 nm, indicating the existence of an α,β-unsaturated ketone group. The ^{1}H NMR data (Table 1) of **1** combined with the data from HSQC showed the existence of proton

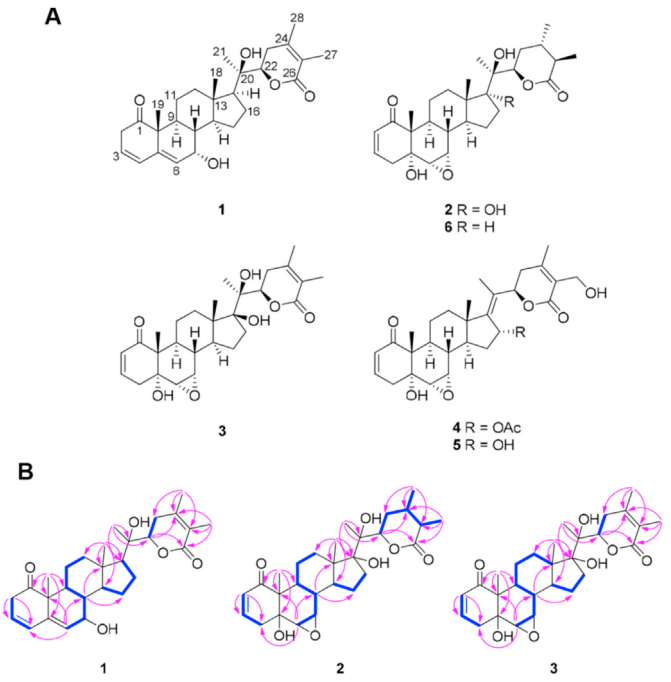

Fig. 1. (A) Chemical structures of withanolides (**1**–**6**). (B) Important HMBC (⟶) and COSY (▬) correlations for compounds **1**–**3**.

signals for five methyls [δ_H 0.90 (3H, s), 1.27 (3H, s), 1.32 (3H, s), 1.86 (3H, s), and 1.93 (3H, s)], six methylenes [δ_H 1.23/1.79 (each 1H, m), 1.35/2.00 (each 1H, m), 1.54/1.97 (each 1H, m, overlap), 1.54/1.97 (each 1H, m, overlap), 2.11/2.37 (each 1H, m), 2.77 (1H, dd, J = 20.0, 4.5 Hz)/3.29 (1H, dd, J = 20.0, 2.5 Hz)], and nine methines [δ_H 1.48 (1H, m), 1.50 (1H, m), 1.51 (1H, m), 2.01 (1H, m), 3.94 (1H, m), 4.19 (1H, dd, J = 13.5, 3.5 Hz), 5.79 (1H, m), 5.80 (1H, d, J = 4.5 Hz), and 6.07 (1H, d, J = 10.5 Hz)]. The ^{13}C NMR data, combined with the results of HSQC/HMBC data analyses, revealed 28 carbon resonance signals that were classified into five methyl groups (δ_C 12.3, 13.4, 18.4, 20.4, and 20.7), six methylenes (δ_C 21.6, 21.8, 23.7, 31.6, 39.5, and 39.7), nine methines (δ_C 33.6, 36.2, 50.1, 54.4, 64.5, 80.7, 125.6, 127.1, and 129.1), and eight non-protonated carbons (δ_C 43.3, 52.8, 75.5, 122.1, 144.7, 149.1, 166.3, and 209.6). Comprehensive scrutiny of the NMR spectral data suggested that the chemical structure of **1** was very similar to that of withasilolide A, previously identified from Indian ginseng, but the apparent difference in the planar structures of **1** and withasilolide A was in the position of the olefinic group in ring A [22]. From the COSY correlations from H_2-2 to H-4 and the key HMBC correlations of H_2-2/C-3, H_2-2/C-4, and H-6/C-4, we deduced that the double bond of C-2/C-3 in withasilolide A was shifted to between C-3 and C-4 in **1**, leading to the formation of the conjugated 3,5-diene system in rings A and B (Fig. 1B). The complete gross structure of **1** was further verified by the detailed inspection of the COSY and HMBC data (Fig. 1B).

The absolute stereochemistry of **1** was determined by examination of the spectrum obtained by ROESY, vicinal proton coupling constants, and data obtained from ECD. The negative Cotton effect at around 304 nm in the ECD data of **1** led to the confirmation of the *trans*-linkage in the A/B ring [26]. ROESY correlations of H_3-19/H-8, H-7/H-8, and H-8/H_3-18 revealed their β-orientation in the partial structure of **1**. Meanwhile, the α-orientations at H-9, H-14, H-17, H_3-21, and H-22 were also confirmed by the ROESY correlations, as depicted in Fig. 2. In particular, the ROESY correlations of H_3-21/H-17 and H_3-21/H-23α determined the *R*-form of the hydroxylated quaternary carbon at C-20. According to the spectroscopic values reported in the previous study, the ^{1}H NMR spectrum of H-22α possesses a doublet of doublets with two different coupling constants (J = 9.0–13.8 and 0.5–4.0 Hz) [22,26], while the ^{1}H NMR spectrum of H-22β shows two similar coupling constants (J = 2.5–7.0, 2.0–5.0 Hz) [27]. Based on the two different coupling constants observed as J = 13.5 and 3.5 Hz, the orientation of H-22 was determined to be α-form, which was also verified by the ROESY correlations of H-16α/H-22 and H-17/H-22. In fact, the absolute configuration of C-22 was unambiguously elucidated to be *R*-form by the positive Cotton effect at 250–260 nm derived from the n → π* transition of the α,β-unsaturated δ-lactone [22,27]. Finally, for the absolute configuration determination of **1**, the ECD data of two possible isomers, **1a** (7*S*,20*R*,22*R*) and **1b** (7*R*,20*S*,22*S*), were subjected to quantum mechanics calculations. The results of calculation of the ECD data revealed that the ECD curve of **1a** (blue line) was consistent with the experimentally determined ECD spectrum of **1** (Fig. 3A). Therefore, the chemical structure of **1** was successfully determined as illustrated in Fig. 1 and its trivial name was withasilolide G.

Compound **2**, isolated as a white powder, had the molecular formula of $C_{28}H_{40}O_7$, based on the data obtained by positive-ion mode HR-ESIMS, exhibiting a protonated ion peak at *m/z* 489.2852 $[M + H]^+$ (calculated for $C_{28}H_{41}O_7$, 489.2852). The ^{1}H and ^{13}C NMR spectral data (Table 1) of **2**, combined with the evidence obtained by HSQC, revealed the presence of a distinctive A/B ring pattern observed in 6α,7α-epoxy-5α-hydroxy-1-oxowitha-2-enolide [21], as determined from the NMR signals at C-1 (δ_C 202.9), C-2 [δ_H 5.82 (1H, dd, J = 10.0 and 2.5 Hz) and δ_C 129.0], and C-3 [δ_H 6.57 (1H, ddd, J = 10.0, 5.0 and 2.0 Hz) and δ_C 139.7] for an α,β-unsaturated ketone; C-5 (δ_C 73.1) for a hydroxylated quaternary carbon; and C-6 [δ_H 3.01 (1H, d, J = 4.0 Hz) and δ_C 56.1] and C-7 [δ_H 3.29 (1H, dd, J = 3.5 and 2.0 Hz) and δ_C 57.0] responsible for an epoxy functional group. The partial structure of **2** was also supported by interpretation of the key HMBC correlations from H-2/C-3, H-3/C-1, H-3/C-5, H_3-19/C-5, H_3-19/C-1 and H-6/C-10, as well as the key COSY correlations from H-2 to H-4 and H-6 to H-9 (Fig. 1B). The existence of two angular methyl units at C-18 [δ_H 0.89 (3H, s) and δ_C 16.2] and C-19 [δ_H 1.15 (3H, s) and δ_C 14.7] and three methyls at C-21 [δ_H 1.24 (3H, s) and δ_C 21.9], C-27 [δ_H 1.21 (3H, d, J = 6.5 Hz) and δ_C 14.0], and C-28 [δ_H 1.11 (3H, d, J = 7.0 Hz) and δ_C 20.9] were also clearly detected in the NMR data of **2**. Moreover, the presence of a 3,4-dimethyltetrahydropyran-2-one moiety was elucidated by the key COSY correlations from H-22 to H-25, and the HMBC correlations for H-22/C-26, H_3-27/C-26, H_3-27/C-24, H_3-28/C-23 and H_3-28/C-25 (Fig. 1B). A thorough analysis of the 2D NMR data of **2** indicated that the NMR spectroscopic values of **2** were quite similar to those of withasilolide C identified from the same natural source in a previous study [22], with the difference of a hydroxyl group at C-20 (δ_C 76.0) in **2**. This inference was verified by important HMBC correlations from H_3-21, H-22, H_2-23 and H_2-16 to C-20 (Fig. 1B), which led to the final structure of **2**.

By comparing the spectroscopic values and analyzing the ROESY experiment and ECD data, the absolute configuration of **2** was elucidated to be identical to that of withasilolide C. The α-position of the epoxy group between C-6 and C-7 was assigned by the ROESY correlations of H-7/H-8, H-6/H-7 and H_3-19/H-8, and the coupling constant of 3.5 Hz between H-6 and H-7 (Fig. 2), which also indicated the *trans*-linkage in the conformation of A/B ring in **2**, because a smaller coupling constant as 0–2 Hz for H-6 is typical in *cis*-linkages [22,26,27]. The *trans*-linkage for the A/B ring was further verified by the key negative Cotton effect around 340 nm in the ECD experiment of **2** [22], and the configurations at C-5, C-6, and C-7 were assigned accordingly, as depicted in Fig. 2. Additionally, the weak positive Cotton effect in the region of 250–260 nm provided critical evidence for confirming the 22*R* configuration [22,27]. The

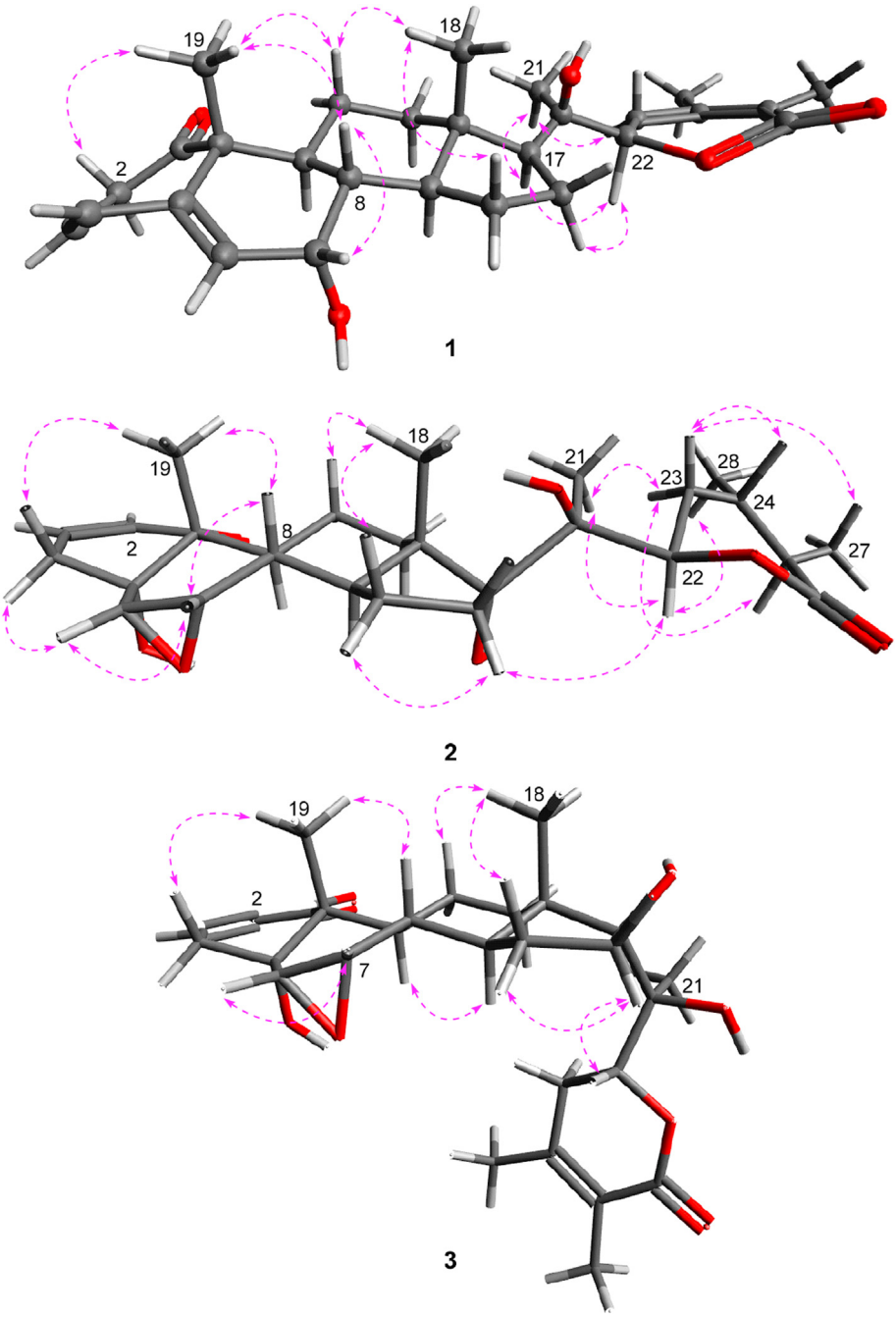

Fig. 2. Important ROESY correlations for compounds **1**–**3**.

stereochemistry of the δ-lactone ring was assigned from the ROESY data analysis (Fig. 2), where the correlations from H-23β to H-24, H-23α to H-25, and H-22 to H_3-28 suggested that H-24 and H-25 were in β- and α-orientations, respectively. H-24 and H-25 were confirmed to be in axial orientation, as revealed by the coupling constant as 9.5 Hz [22]. The negative Cotton effect at around 220 nm in the ECD experiment supported the half-chair confirmation of the saturated δ-lactone of **2** [22,27], which indicated a configuration of 22*R*,24*S*,25*R*. Considering the ROESY correlations from H-22 and H-23α to H_3-21, the chiral center at C-20 was determined to be in *S*-form (Fig. 2). In a previous study, ^{13}C NMR γ-gauche effects on the carbon chemical shifts of C-18 and C-12, as well as C-21 were used for distinguishing epimeric withanolides with OH-17α and OH-17β groups [22,27]. The ^{13}C NMR data of the epimers of 17-hydroxywithanolides indicated that the alteration in the OH-17 orientation from β to α induced an upfield shift in the C-12 and C-18 chemical shifts, but a downfield shift in the C-21 chemical shift in the same $CDCl_3$ solvent owing to the γ-gauche effects of the OH-17 group [27]. The differences in the C-12, C-18, and C-21 carbon chemical shifts were determined for identifying the stereochemistry at C-17. The differences between **2** and philadelphicalactone C were $\Delta\delta_{C\text{-}12}$ (+0.8 ppm), $\Delta\delta_{C\text{-}18}$ (+0.4 ppm), and $\Delta\delta_{C\text{-}21}$ (−-0.1 ppm), while the differences between **2** and 17-*epi*-philadelphicalactone A were $\Delta\delta_{C\text{-}12}$ (−0.9 ppm), $\Delta\delta_{C\text{-}18}$ (−0.5 ppm), and $\Delta\delta_{C\text{-}21}$ (+2.0 ppm) in the same $CDCl_3$ solvent. These results provided significant evidence that the absolute stereochemistry of

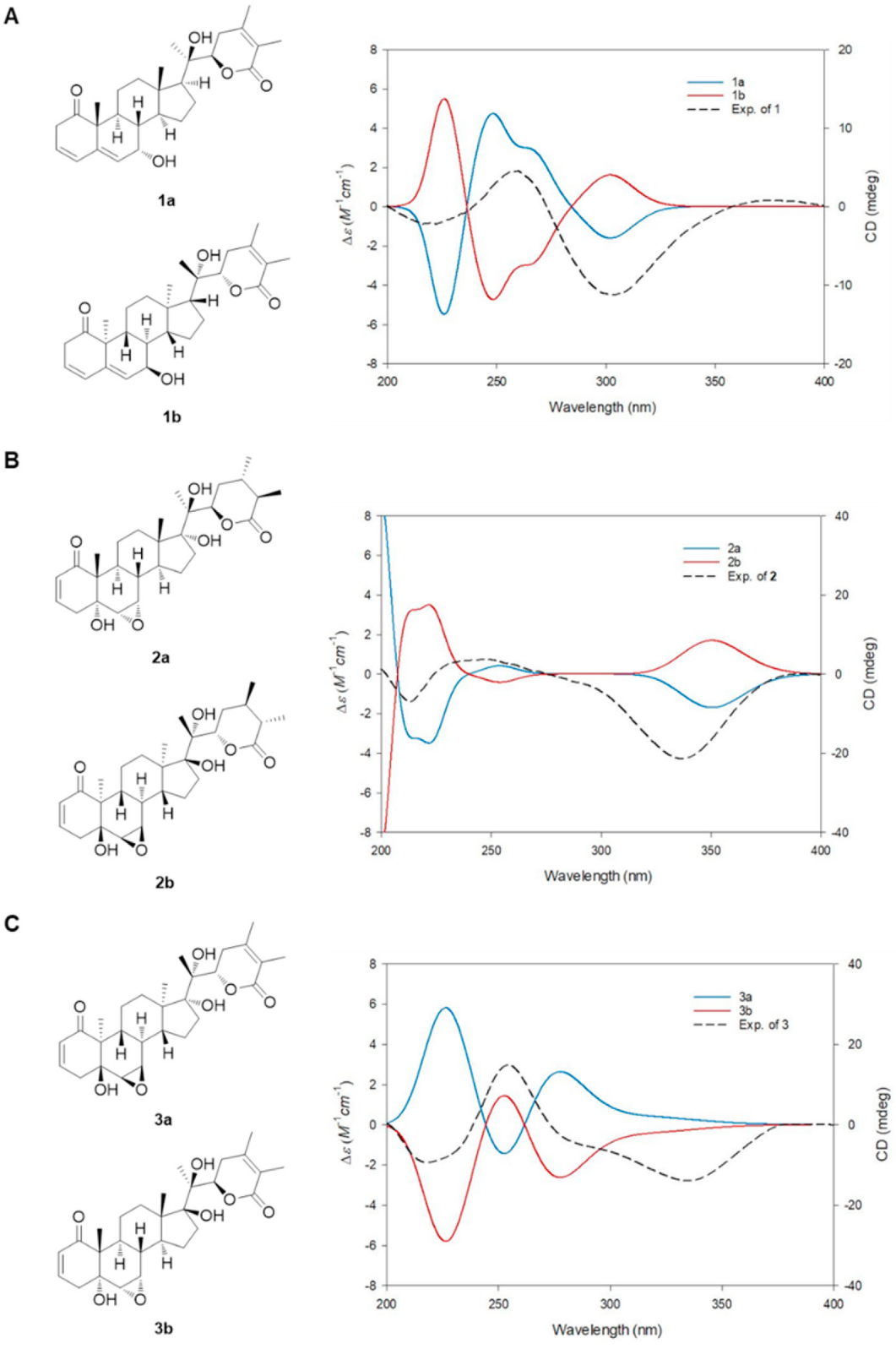

Fig. 3. Experimental and computed ECD data of compound (A) **1**, (B) **2** and (C) **3**.

C-17 was the *R*-form [27]. Additionally, the proton chemical shifts of H_2-12, H_3-18, and H-21 of **2** were similar to those of the 17α-hydroxywithanolide, philadelphicalactone C [27]. To prove this assignment, the NMR chemical shifts of 17*R*-**2** and 17*S*-**2** as the two possible diastereomers were calculated, and the calculated NMR chemical shifts were empirically scaled for removing system errors, which is a common practice in such calculations [28–30]. The calculated NMR chemical shifts of 17*R*-**2**/17*S*-**2** and the

experimental values obtained for **2** were compared. The differences ($\Delta\delta$) were resolved based on the formula $\Delta\delta = \delta_{calcd} - \delta_{exptl}$ and are accessible in Table S1 (Supplementary data). The correlation coefficient (R^2) obtained by linear regression analysis, largest absolute deviation (LAD), and the mean absolute deviation (MAD) for 17*R*-**2** were 0.9970 (Fig. 4A), 3.96, and 0.99 (Fig. 4B), respectively, while the R^2, LAD, and MAD values for 17*S*-**2** were 0.9965, 5.73, and 1.18, respectively, which indicated that the structure of 17*R*-**2** was highly accurate and consistent with the 17*R* assignment determined by NMR analysis. For its absolute stereochemistry, an experiment for ECD calculations were achieved by comparing the experimental ECD data of **2** with the computed ECD data of **2a** (17*R*,20*S*,22*R*,24*S*,25*R*) and **2b** (17*S*,20*R*,22*S*,24*R*,25*S*) as the two possible enantiomers (Fig. 3B). The experimental data of **2** showed good correlation with the computed curve of **2a**. Accordingly, the chemical structure of **2** was determined to be (17*R*,20*S*,22*R*,24*S*,25*R*)-6α,7α-epoxy-5α,17,20-trihydroxy-1-oxowitha-2-enolide and the trivial name was withasilolide H.

Compound **3**, obtained as a white powder showed the HR-ESIMS data displaying a protonated ion peak at *m/z* 487.2689 $[M + H]^+$ (calculated for $C_{28}H_{39}O_7$, 487.2696), which suggested the molecular formula of $C_{28}H_{38}O_7$. The NMR spectral data (Table 1) of **3** contained signals similar to those of **2**, with the exception of the signals corresponding to the double bond of C-24 (δ_C 150.7)/C-25 (δ_C 120.9) in **3**. The partial structure of the δ-lactone ring was verified by the key HMBC correlations of H-22/C-24, H_3-27/C-24, H_3-27/C-26, H_3-27/C-25, H_3-28/C-24, H_3-28/C-23 and H_3-28/C-25 (Fig. 1B), which verified the complete planar structure of **3** as depicted in Fig. 1B.

The stereochemistry of **3** was also established using the ROESY data, proton coupling constants, ECD calculations**,** and NMR chemical shifts calculations. Overall, the stereochemistry of **3** was identical to that of **2** because most of the data, including the ROESY and ECD data, and the characteristic *J* values were identical to those of compound **2**. However, there were noticeable differences in the signals corresponding to C-17 (δ_C 87.0 for **3**; δ_C 89.4 for **2**), which indicated that the chirality of C-17 differed between compounds **2** and **3**. For the stereochemistry at C-17 in **3**, the NMR spectroscopic values of the related withanolides were compared. As aforementioned, the key chemical shifts in the ^1H and ^{13}C NMR spectra for C-12 and C-18 were relatively deshielded, but those of C-21 were shifted upfield by the presence of the 17β-hydroxy group, compared to those of the 17α-hydroxy group [27]. This difference was distinct between compounds **2** and **3** as compound **2** is a 17α-hydroxywithanolide. The differences in the ^{13}C NMR chemical shifts of **2** and **3** ($\Delta = \delta_{\mathbf{2}} - \delta_{\mathbf{3}}$) were −0.7, −1.0, and +2.0 ppm for C-12, C-18, and C-21, respectively, which confirmed the absolute configuration of C-17 in **3** to be *S*-form. To elucidate the absolute configuration of C-17, NMR chemical shifts of 17*R*-**3** and 17*S*-**3** as the two possible diastereomers were calculated, and the NMR chemical shifts of 17*R*-**3** and 17*S*-**3** that had been calculated computationally were compared with the corresponding experimentally determined values for **3**. The differences ($\Delta\delta$) were calculated (Table S2, Supplementary data), and the results showed that the values of R^2, LAD, and MAD were 0.9983 (Fig. 4C), 6.35 and 1.08 (Fig. 4D), respectively, for 17*R*-**3**, and 0.9986, 4.14, and 0.95, respectively, for 17*S*-**3**. The results indicated that the 17*S*-**3** form was more reasonable, as it agreed with the 17*S* assignment determined by NMR analysis. Finally, the experimental ECD curve of **3** agreed with the computed ECD spectrum for **3b** (17*S*,20*S*,22*R*) rather than with that of **3a** (17*R*,20*R*,22*S*) (Fig. 3C). Consequently, the chemical structure of **3** was finally elucidated as shown in Fig. 1 and the trivial name was withasilolide I.

By comparing the NMR spectroscopic data obtained herein with those previously reported in literatures [22,23] along with LC/MS analysis, we identified 3 known withanolides in this study, namely, withasilolide F (**4**), withasilolide E (**5**), and withasomniferol B (**6**).

3.3. Evaluation of the anti-adipogenic activity of the isolated compounds

Obesity is a major health problem that is caused by the summation of multiple factors, including genetic, dietary, lifestyle-related, and environmental factors, which lead to the excessive accumulation of body fat in the adipose tissues [31]. The growth of adipose tissues occurs with the differentiation of preadipocytes in the adipose tissues into adipocytes, and the generation and accumulation of lipid droplets in the adipocytes [32,33]. Therefore, the discovery of active compounds that prevent adipogenesis and lipogenesis has been considered to be a potential therapeutic strategy for the prevention of obesity and metabolic diseases, which has attracted attention to the discovery of natural compounds with anti-adipogenic potential.

Before assessing the effect of compounds **1**–**6** on adipogenesis, the 3T3-L1 preadipocytes were treated with all the compounds at different concentrations of 0, 12.5, and 25 μM for 24 h, for evaluating their cytotoxicity in the 3T3-L1 preadipocytes. None of the compounds caused cytotoxic effects at concentrations of up to 25 μM (Figure S22). Therefore, the 3T3-L1 cells were treated with the compounds **1**–**6** during adipogenesis at a concentration of 25 μM, for evaluating their anti-adipogenic activities in the subsequent experiments. After 10 days of differentiation, the lipid droplets within the mature adipocytes were stained using Oil Red O working solution [34]. Microscopic examination of the stained adipocytes revealed that compounds **1**–**6** significantly inhibited adipogenesis and suppressed the enlargement of lipid droplets compared to those of the control setup (Fig. 5B). Furthermore, the mRNA expression levels of *Fabp4* and *Adipsin*, the adipocyte marker genes were markedly reduced following treatment with 25 μM of compounds **1**–**6** (Fig. 5C). To assess dose-dependent response of one of the effective compounds, we evaluated the protein level of A-FABP, an adipogenic marker, according to the treatment with diverse concentrations of compound **2**, which was a sufficient amount of the new compound for further evaluation. The immunoblot data showed that treatment with compound **2** reduced the protein level of A-FABP in dose-dependent manner (Fig. 5D). These results indicated that the compounds **1**–**6** alleviated adipogenesis in the 3T3-L1 preadipocytes.

As compounds **1**–**6** were able to suppress adipogenesis, we investigated whether they were capable of controlling lipid metabolism (Fig. 5E-G). The effects of compounds **1**–**6** on lipolysis and lipogenesis were measured by determining the difference in the ratio of expression of the lipolytic genes (*HSL* and *ATGL*) to the lipogenic gene (*SREBP1*) and comparing with that of the control. The mRNA expression of *HSL* and *ATGL,* the lipolytic genes in the 3T3-L1 cells was upregulated by treatment with compounds **1**–**5**; however, the mRNA expression of *ATGL* was not upregulated by compound **6** (Fig. 5E and F). On the other hand, the mRNA expression of *SREBP1*, the lipogenic gene was downregulated following treatment with 25 μM of compounds **1**–**6** during adipogenesis (Fig. 5G). These data demonstrated that compounds **1**–**6** can enhance lipid metabolism by promoting lipolysis and inhibiting lipogenesis.

4. Conclusions

In conclusion, we identified 6 withanolides, including 3 novel withanolides, withasilolides G–I (**1**–**3**), from a MeOH extract of Indian ginseng roots by LC/MS. The effects of compounds **1**–**6** on lipid metabolism and adipogenesis were evaluated during

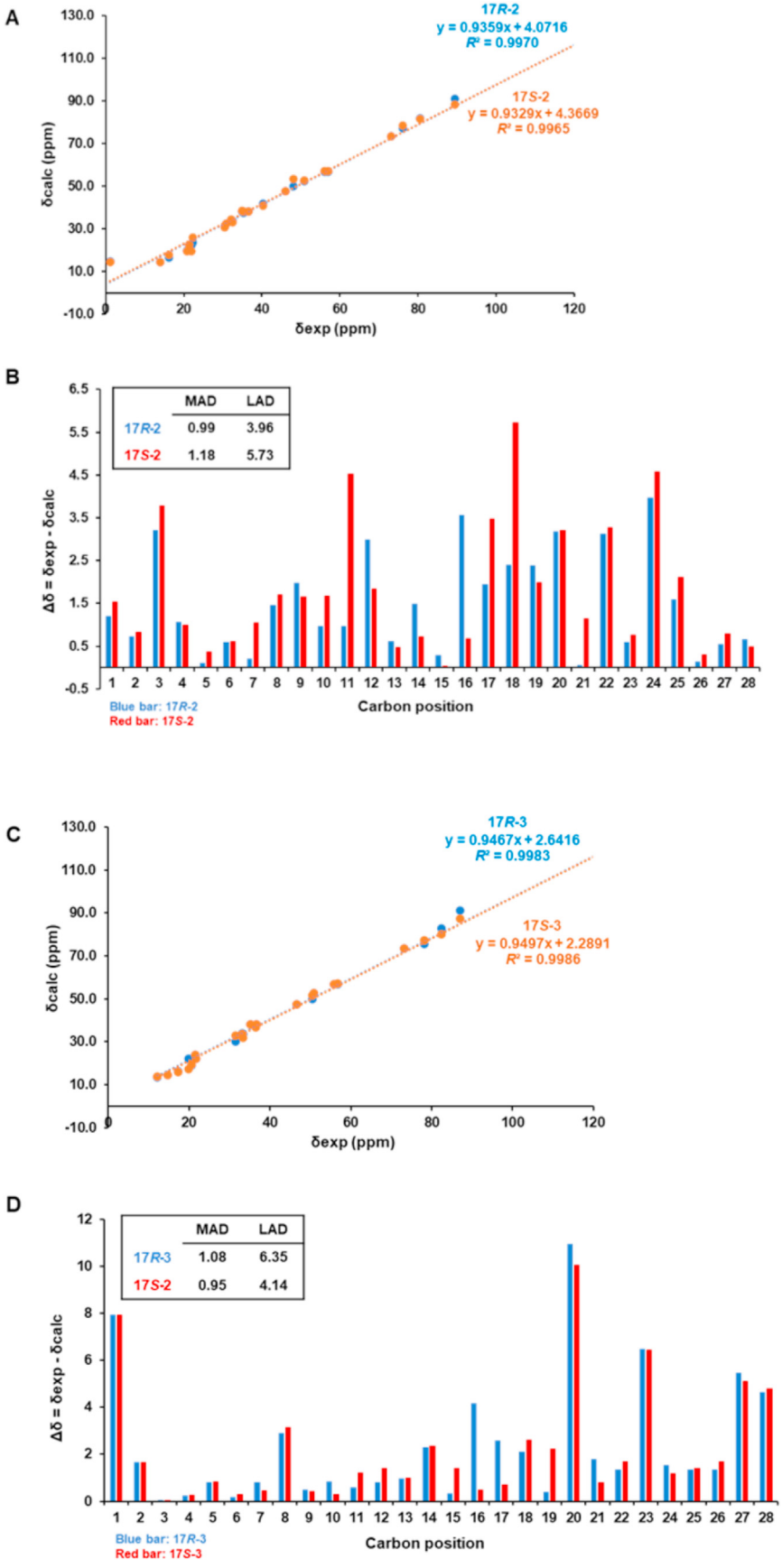

Fig. 4. (A) Regression analysis of the experimental versus computed ^{13}C NMR chemical shifts of 17*R*-**2** and 17*S*-**2**. (B) Relative chemical shift errors between the computed and experimental ^{13}C NMR data for 17*R*-**2** and 17*S*-**2**. (C) Regression study of the experimental versus computed ^{13}C NMR chemical shifts of 17*R*-**3** and 17*S*-**3**. (D) Relative chemical shift errors between the computed and experimental ^{13}C NMR data for 17*R*-**3** and 17*S*-**3**.

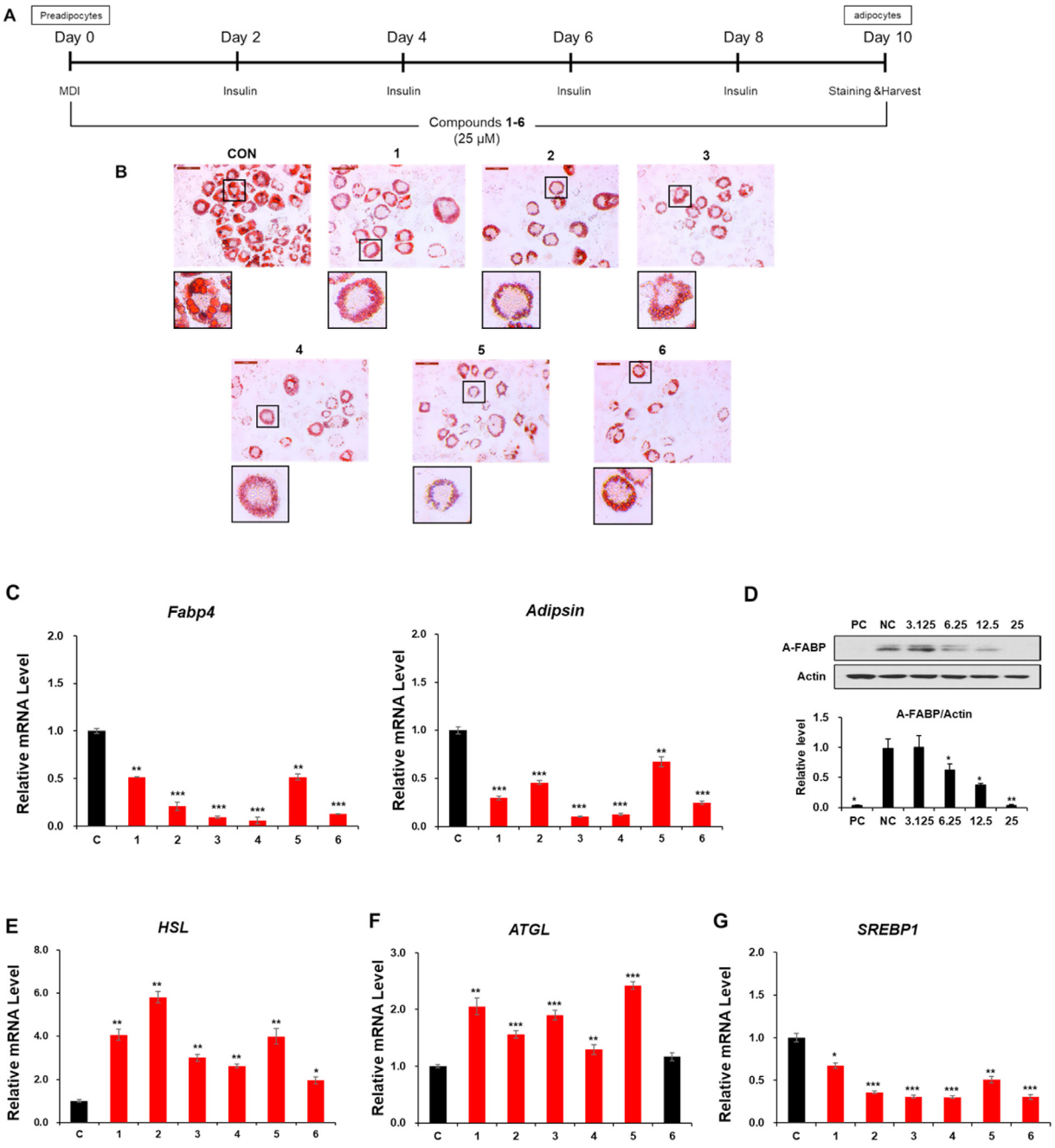

Fig. 5. Inhibitory effects of the compounds **1**–**6** on adipogenesis. (A) Schematic representation of the differentiation of 3T3-L1 preadipocytes into adipocytes following 10 days of culture. The 3T3-L1 cells were treated with the compounds **1**–**6** during differentiation (B) Images of adipocytes stained with Oil Red O following incubation with 25 μM of compounds **1**–**6** during adipogenesis. (C) The relative mRNA expression of *Fabp4* and *Adipsin* in 3T3-L1 adipocytes incubated with 25 μM of compounds **1**–**6** during adipogenesis. The inhibitory effects of compounds **1**–**6** on lipid metabolism. (D) Immunoblot data of 3T3-L1 adipocytes incubated with 30 μM of resveratrol as a positive control (PC), DMSO as a negative control (NC) and indicated concentrations of compound **2**. (E–G) The relative mRNA expression of *HSL* (E), *ATGL* (F), and *SREBP1* (G) in 3T3-L1 adipocytes incubated with 25 μM of the compounds **1**–**6** during adipogenesis. The data are presented as the mean ± SEM of n = 3 replicates. Statistical significance was compared to control (C, E-G) or negative control (D). *$p < 0.05$, **$p < 0.01$, and ***$p < 0.001$.

adipocyte maturation. Compounds **1**–**6** effectively inhibited the differentiation of 3T3-L1 preadipocytes to adipocytes by reducing the mRNA expression levels of *Fabp4* and *Adipsin*. We also observed that compounds **1**–**6** regulated lipid metabolism by upregulating the expression of *ATGL* and *HSL*, the lipolytic genes and down-regulating the expression of *SREBP1*, the lipogenic gene. The results of our experimental studies demonstrated the anti-adipogenic activity of compounds **1**–**6**, and we propose that these compounds have the potential to prevent adipogenesis in obesity, and can suppress excessive lipid accumulation in obesity-related metabolic disorders.

Declaration of competing interest

The authors declare no conflicts of interest.

Acknowledgments

This work was supported by a grant from the National Research Foundation of Korea (NRF), funded by the Korean government (MSIT) (grant number: 2019R1A5A2027340 and 2021R1A2C2007937).

Appendix A. Supplementary data

Supplementary data to this article can be found online at https://doi.org/10.1016/j.jgr.2021.09.004.

References

[1] Jayaprakasam B, Zhang Y, Seeram NP, Nair MG. Growth inhibition of human tumor cell lines by withanolides from *Withania somnifera* leaves. Life Sci 2003;74:125–32.
[2] Choudhary MI, Yousuf S, Nawaz SA, Ahmed S, Atta R. Cholinesterase inhibiting withanolides from *Withania somnifera*. Chem Pharm Bull 2004;52:1358–61.
[3] Mary NK, Babu BH, Padikkala J. Antiatherogenic effect of Caps HT2, a herbal Ayurvedic medicine formulation. Phytomedicine 2003;10:474–82.
[4] Gupta GL, Rana AC. PHCOG MAG.: plant review *Withania somnifera* (Ashwagandha): a review. Phcog Rev 2007;1:129–36.
[5] Srivastava A, Gupta AK, Shanker K, Gupta MM, Mishra R, Lal RK. Genetic variability, associations, and path analysis of chemical and morphological traits in Indian ginseng [*Withania somnifera* (L.) Dunal] for selection of higher yielding genotypes. J Ginseng Res 2018;42:128–64.
[6] Ganguly B, Kumar N, Ahmad AH, Rastogi SK. Influence of phytochemical composition on in vitro antioxidant and reducing activities of Indian ginseng [*Withania somnifera* (L.) Dunal] root extracts. J Ginseng Res 2018;42:463–9.
[7] Singh S, Kumar S. *Withania somnifera*. The Indian ginseng ashwagandha. Lucknow, India: Central Institute of Medicinal and Aromatic Plants; 1998.
[8] Atta-ur-Rahman YM, Gul W, Qureshi S, Choudhary MI, Voelter W, Hoff A, Jens F, Naz A. Cholinesterase inhibiting withanolides from *Withania somnifera*. Heterocycles 1998;48:1801–11.
[9] Bhattacharya SK, Satyan KS, Chakrabarti A. Effect of Trasina, an Ayurvedic herbal formulation, on pancreatic islet superoxide dismutase activity in hyperglycaemic rats. Indian J Exp Biol 1997;35:297–9.
[10] Dhuley JN. Effect of ashwagandha on lipid peroxidation in stress-induced animals. J Ethnopharmacol 1998;60:173–8.
[11] Bhattacharya A, Ramanathan M, Ghosal S, Bhattacharya SK. Effect of *Withania somnifera* glycowithanolides on iron-induced hepatotoxicity in rats. Phytother Res 2000;14:568–70.
[12] Kulkarni SK, Verma A. Prevention of development of tolerance and dependence to opiate in mice by BR-16A (Mentat ®), a herbal psychotropic preparation. Indian J Exp Biol 1992;30:885–8.
[13] Ganzera M, Choudhary MI, Khan IA. Quantitative HPLC analysis of withanolides in *Withania somnifera*. Fitoterapia 2003;74:68–76.
[14] Elsakka M, Grigorescu E, Stanescu U, Stanescu U, Dorneanu V. New data referring to chemistry of *Withania somnifera* species. Rev Med-Chir Soc Med Nat Iasi 1990;94:385–7.
[15] Matsuda H, Murakami T, Kishi A, Yoshikawa M. Structures of withanosides I, II, III, IV, V, VI and VII new withanolide glycosides from the roots of Indian *Withania somnifera* D and inhibitory activity for tachyphylaxis to clonidine in isolated guineapig ileum. Bioorg Med Chem 2001;96:1499–507.
[16] Davis L, Kuttan G. Immunomodulatory activity of *Withania somnifera*. J Ethnopharmacol 2000;71:193–200.
[17] Park HJ, Rayalam S, Della-Fera MA, Ambati S, Yang JY, Baile CA. Withaferin A induces apoptosis and inhibits adipogenesis in 3T3-L1 adipocytes. Biofactors 2008;33:137–48.
[18] Lee S, Ryoo R, Choi JH, Kim JH, Kim SH, Kim KH. Trichothecene and tremulane sesquiterpenes from a hallucinogenic mushroom *Gymnopilus junonius* and their cytotoxicity. Arch Pharm Res (Seoul) 2020;43:214–23.
[19] Ha JW, Kim J, Kim H, Jang W, Kim KH. Mushrooms: an important source of natural bioactive compounds. Nat Prod Sci 2020;26:118–31.
[20] Lee SR, Kang H, Yoo MJ, Yu JS, Lee S, Yi SA, Beemelmanns C, Lee J, Kim KH. Anti-adipogenic pregnane steroid from a *Hydractinia*-associated fungus, *Cladosporium sphaerospermum* SW67. Nat Prod Sci 2020;26:230–5.
[21] Yu JS, Park M, Pang C, Rashan L, Jung WH, Kim KH. Antifungal phenols from *Woodfordia uniflora* collected in Oman. J Nat Prod 2020;83:2261–8.
[22] Kim S, Yu JS, Lee JY, Choi SU, Lee J, Kim KH. Cytotoxic withanolides from the roots of Indian ginseng (*Withania somnifera*). J Nat Prod 2019;82:765–73.
[23] Baek SC, Lee S, Kim S, Jo MS, Yu JS, Ko YJ, Cho YC, Kim KH. Withaninsams A and B: phenylpropanoid esters from the roots of Indian ginseng (*Withania somnifera*). Plants 2019;8:527.
[24] Yu JS, Li C, Kwon M, Oh T, Lee TH, Kim DH, Ahn JS, Ko SK, Kim CS, Cao S, Kim KH, Herqueilenone A. A unique rearranged benzoquinone-chromanone from the Hawaiian volcanic soil-associated fungal strain *Penicillium herquei* FT729. Bioorg Chem 2020;105:104397.
[25] Lee SR, Lee D, Park M, Lee JC, Park HJ, Kang KS, Kim CE, Beemelmanns C, Kim KH. Absolute configuration and corrected NMR assignment of 17-hydroxycyclooctatin, a fused 5-8-5 tricyclic diterpene. J Nat Prod 2020;83:354–61.
[26] Kuroyanagi M, Shibata K, Umehara K. Cell differentiation inducing steroids from *Withania somnifera* L.(Dun.). Chem Pharm Bull 1999;47:1646–9.
[27] Xu YM, Wijeratne EMK, Brooks AD, Tewary P, Xuan LJ, Wang WQ, Sayers TJ, Gunatilaka AAL. Cytotoxic and other withanolides from aeroponically grown *Physalis philadelphica*. Phytochemistry 2018;152:174–81.
[28] Smith SG, Goodman JM. Assigning the stereochemistry of pairs of diastereoisomers using GIAO NMR shift calculation. J Org Chem 2009;74:4597–607.
[29] Smith SG, Goodman JM. Assigning stereochemistry to single diastereoisomers by GIAO NMR calculation: the DP4 probability. J Am Chem Soc 2010;132:12946–59.
[30] Hehre W, Klunzinger P, Deppmeier B, Driessen A, Uchida N, Hashimoto M, Fukushi E, Takata Y. Efficient protocol for accurately calculating ^{13}C chemical shifts of conformationally flexible natural products: scope, assessment, and limitations. J Nat Prod 2019;82:2299–306.
[31] Spiegelman BM, Flier JS. Obesity and the regulation of energy balance. Cell 2001;104:531–43.
[32] Smith U, Kahn BB. Adipose tissue regulates insulin sensitivity: role of adipogenesis, de novo lipogenesis and novel lipids. J Intern Med 2016;280:465–75.
[33] Lee K, Seo YJ, Song JH, Chei S, Lee BY. Ginsenoside Rg1 promotes browning by inducing UCP1 expression and mito-chondrial activity in 3T3-L1 and subcutaneous white adipocytes. J Ginseng Res 2019;43:589–99.
[34] Yi SA, Lee J, Park SK, Kim JY, Park JW, Lee MG, Nam KH, Park JH, Oh H, Kim S, Han J, Kim BK, Jo DG, Han JW. Fermented ginseng extract, BST204, disturbs adipogenesis of mesenchymal stem cells through inhibition of S6 kinase 1 signaling. J Ginseng Res 2020;44:58–66.